

MuseGNN: Interpretable and Convergent Graph Neural Network Layers at Scale

Haitian Jiang¹
haitian.jiang@nyu.edu*

Renjie Liu²
liurj2023@mail.sustech.edu.cn

Xiao Yan²
yanx@sustech.edu.cn

Zhenkun Cai³
zkcai@amazon.com

Minjie Wang³
minjiw@amazon.com

David Wipf³
david.wipf@gmail.com[†]

¹New York University

²Southern University of Science and Technology

³AWS Shanghai AI lab

Abstract

Among the many variants of graph neural network (GNN) architectures capable of modeling data with cross-instance relations, an important subclass involves layers designed such that the forward pass iteratively reduces a graph-regularized energy function of interest. In this way, node embeddings produced at the output layer dually serve as both predictive features for solving downstream tasks (e.g., node classification) and energy function minimizers that inherit desirable inductive biases and interpretability. However, scaling GNN architectures constructed in this way remains challenging, in part because the convergence of the forward pass may involve models with considerable depth. To tackle this limitation, we propose a sampling-based energy function and scalable GNN layers that iteratively reduce it, guided by convergence guarantees in certain settings. We also instantiate a full GNN architecture based on these designs, and the model achieves competitive accuracy and scalability when applied to the largest publicly-available node classification benchmark exceeding 1TB in size.

1 Introduction

Graph neural networks (GNNs) are a powerful class of deep learning models designed specifically for graph-structured data. Unlike conventional neural networks that primarily operate on independent samples, GNNs excel in capturing the complex cross-instance relations modeled by graphs [Hamilton et al., 2017, Kearnes et al., 2016, Kipf and Welling, 2017, Velickovic et al., 2018]. Foundational to GNNs is the notion of message passing [Gilmer et al., 2017], whereby nodes iteratively gather information from neighbors to update their representations. In doing so, information can propagate across the graph in the form of node embeddings, reflecting both local patterns and global network effects, which are required by downstream tasks such as node classification.

Among many GNN architectures, one promising subclass is based on graph propagation layers derived to be in a one-to-one correspondence with the descent iterations of a graph-regularized energy function [Chen et al., 2022, Ahn et al., 2022, Yang et al., 2021, Ma et al., 2021, Gasteiger et al., 2019, Pan et al., 2020, Zhang et al., 2020, Zhu et al., 2021, Xue et al., 2023]. For these models, the layers of the GNN forward pass computes increasingly-refined approximations to a minimizer of the aforementioned energy. Importantly, if such energy minimizers possess interpretable/explainable properties or inductive biases, the corresponding GNN architecture naturally inherits them, unlike traditional GNN constructions that may be less transparent. More broadly, this association between the GNN forward pass and optimization can be exploited to introduce targeted architectural enhancements (e.g., forming explainable predictions, robustly handling graphs with spurious edges, etc.). Borrowing from [Chen and Eldar, 2021, Yang et al., 2022], we

*Work done during internship at AWS Shanghai AI lab.

[†]Corresponding to David Wipf.

will henceforth refer to models of this genre as *unfolded* GNNs, given that the layers are derived from a so-called unfolded (in time/iteration) energy descent process.

Despite their merits w.r.t. interpretability, unfolded GNNs face non-trivial scalability challenges. This is in part because they can be constructed with arbitrary depth (i.e., arbitrary descent iterations) while still avoiding undesirable oversmoothing effects [Oono and Suzuki, 2020, Li et al., 2018], and the computational cost and memory requirements of this flexibility are often prohibitively high. Even so, there exists limited prior work explicitly tackling the scalability of unfolded GNNs, or providing any complementary guarantees regarding convergence on large graphs. Hence most unfolded GNN models are presently evaluated on relatively small benchmarks.

To address these shortcomings, we propose a scalable unfolded GNN model that incorporates efficient subgraph sampling within the fabric of the requisite energy function. Our design of this model is guided by the following three desiderata: (i) maintain the characteristic interpretable properties and extensible structure of full-graph unfolded GNN models, (ii) using a consistent core architecture, preserve competitive accuracy across datasets of varying size, including the very largest publicly-available benchmarks, and (iii) do not introduce undue computational or memory overheads beyond what is required to train the most common GNN alternatives. Our proposed model, which we will later demonstrate satisfies each of the above, is termed *MuseGNN* in reference to a GNN architecture produced by the *minimization* of an *unfolded sampling-based energy*. Building on background motivations presented in Section 2, our MuseGNN-related contributions herein are three-fold:

- In Sections 3 and 4, we expand a widely-used unfolded GNN framework to incorporate offline sampling into the architecture-inducing energy function design itself, as opposed to a post hoc application of sampling to existing GNN methods. The resulting model, which we term MuseGNN, allows us to retain the attractive interpretability and extensibility properties of unfolded GNNs, with the scalability of canonical GNN architectures.
- We analytically demonstrate in Section 5 that MuseGNN possesses desirable convergence properties regarding both upper-level (traditional model training) and lower-level (interpretable energy function descent) optimization processes. In doing so we increase our confidence in reliable performance when moving to new problem domains that may deviate from known benchmarks.
- Finally, in Section 6 we provide complementary empirical support that MuseGNN performance is stable in practice, preserving competitive accuracy and scalability across task size. En route, we achieve SOTA performance w.r.t. homogeneous graph models applied to the largest, publicly-available node classification datasets from OGB and IGB exceeding 1TB.

2 Background and Motivation

This section provides background details regarding existing unfolded GNN architectures. Later, we discuss why GNNs formed in this way are relevant, followed by their scalability challenges.

2.1 Interpretable GNN Architectures from Unfolded Optimization

Notation. Let $\mathcal{G} = \{\mathcal{V}, \mathcal{E}\}$ denote a graph with $n = |\mathcal{V}|$ nodes and edge set \mathcal{E} . We define D and A as the degree and adjacency matrices of \mathcal{G} such that the corresponding graph Laplacian is $L = D - A$. Furthermore, associated with each node is both a d -dimensional feature vector, and a d' -dimensional label vector, the respective collections of which are given by $X \in \mathbb{R}^{n \times d}$ and $T \in \mathbb{R}^{n \times d'}$.

GNN Basics. Given a graph defined as above, canonical GNN architectures are designed to produce a sequence of node-wise embeddings $\{Y^{(k)}\}_{k=1}^K$ that are increasingly refined across K model layers according to the rule $Y^{(k)} = h(Y^{(k-1)}; W, A, X) \in \mathbb{R}^{n \times d}$. Here h represents a function that updates $Y^{(k-1)}$ based on trainable model weights W as well as A (graph structure) and optionally X (input node features). To facilitate downstream tasks such as node classification, W may be trained, along with additional parameters θ of any application-specific output layer $g: \mathbb{R}^d \rightarrow \mathbb{R}^{d'}$, to minimize a loss of the form

$$\mathcal{L}(W, \theta) = \sum_{i=1}^{n'} \mathcal{D} \left(g \left[Y^{(K)}(W)_i; \theta \right], T_i \right). \quad (1)$$

In this expression, $Y_i^{(K)} \equiv Y^{(K)}(W)_i$ reflects the explicit dependency of GNN embeddings on W and the subscript i denotes the i -th row of a matrix. Additionally, n' refers to the number of nodes in \mathcal{G} available for training, while \mathcal{D} is a discriminator function such as cross-entropy. We will sometimes refer to the training loss (1) as an *upper-level* energy function to differentiate its role from the lower-level energy defined next.

Moving to Unfolded GNNs. An *unfolded* GNN architecture ensues when the functional form of h is explicitly chosen to align with the update rules that minimize a second, *lower-level* energy function denoted as $\ell(Y)$. In this way, it follows that $\ell(Y^{(k)}) = \ell(h[Y^{(k-1)}; W, A, X]) \leq \ell(Y^{(k-1)})$. This restriction on h is imposed to introduce desirable inductive biases on the resulting GNN layers that stem from properties of the energy ℓ and its corresponding minimizers (see Section 2.2).

While there are many possible domain-specific choices for $\ell(Y)$ in the growing literature on unfolded GNNs [Chen et al., 2022, Ahn et al., 2022, Yang et al., 2021, Ma et al., 2021, Gasteiger et al., 2019, Pan et al., 2020, Zhang et al., 2020, Zhu et al., 2021, Xue et al., 2023]., we will focus our attention on a particular form that encompasses many existing works as special cases, and can be easily generalized to cover many others. Originally inspired by Zhou et al. [2003] and generalized by Yang et al. [2021] to account for node-wise nonlinearities, we consider

$$\ell(Y) := \|Y - f(X; W)\|_F^2 + \lambda \text{tr}(Y^\top LY) + \sum_{i=1}^n \zeta(Y_i), \quad (2)$$

where $\lambda > 0$ is a trade-off parameter, f represents a trainable base model parameterized by W (e.g., a linear layer or MLP), and the function ζ denotes a (possibly non-smooth) penalty on individual node embeddings. The first term in (2) favors embeddings that resemble the input features as processed by the base model, while the second encourages smoothness across graph edges. And finally, the last term is included to enforce additional node-wise constraints (e.g., non-negativity).

We now examine the form of h that can be induced when we optimize (2). Although ζ may be non-smooth and incompatible with vanilla gradient descent, we can nonetheless apply proximal gradient descent in such circumstances [Combettes and Pesquet, 2011], leading to the descent update

$$Y^{(k)} = h \left(Y^{(k-1)}; W, A, X \right) = \text{prox}_\zeta \left(Y^{(k-1)} - \alpha \left[(I + \lambda L)Y^{(k-1)} - f(X; W) \right] \right), \quad (3)$$

where α controls the learning rate and $\text{prox}_\zeta(u) := \arg \min_y \frac{1}{2} \|u - y\|_2^2 + \zeta(y)$ denotes the proximal operator of ζ . Analogous to more traditional GNN architectures, (3) contains a ζ -dependent nonlinear activation applied to the output of an affine, graph-dependent filter. With respect to the former, if ζ is chosen as an indicator function that assigns an infinite penalty to any embedding less than zero, then prox_ζ reduces to standard ReLU activations; we will adopt this choice for MuseGNN.

2.2 Why Unfolded GNNs?

There are a variety of reasons why it can be advantageous to construct h using unfolded optimization steps as in (3) or related. Of particular note here, unfolded GNN node embeddings inherit interpretable characteristics of the lower-level energy, especially if K is sufficiently large such that $Y^{(K)}$ approximates a minimum of $\ell(Y)$. For example, it is well-known that an oversmoothing effect can sometimes cause GNN layers to produce node embeddings that converge towards a non-informative constant [Oono and Suzuki, 2020, Li et al., 2018]. However, it is transparent how to design $\ell(Y)$ such that minimizers do not degenerate in this way, and hence the induced h as in (3) can be iterated indefinitely without risk of oversmoothing, even while spreading information across the graph.

As another representative scenario, in many customer-facing applications, it is desirable to provide explanations for why a particular prediction was made by a GNN model [Ying et al., 2019]. In these situations, the embeddings of unfolded GNNs contain additional information when contextualized w.r.t. their role in

the lower-level energy. For example, if for some node $Y_i^{(K)}$ is very far from $f(X_i; W)$ relative to other nodes, it increases our confidence that subsequent predictions may be based on network effects rather than the local feature X_i . More broadly, the interpretability of unfolded GNNs facilitates bespoke modifications of (3) for addressing heterophily and/or adversarial attacks [Yang et al., 2021], handling long-range dependencies [Xue et al., 2023], forming connections with the gradient dynamics of physical systems [Di Giovanni et al., 2023] and deep equilibrium models [Gu et al., 2020, Yang et al., 2022], and exploiting the robustness of boosting algorithms [Sun et al., 2019] among other things.

2.3 Scalability Challenges and Candidate Solutions

As benchmarks continue to expand in size (see Table 1 below), it is no longer feasible to conduct full-graph GNN training using only a single GPU or even single machine, especially so for relatively deep unfolded GNNs. To address such GNN scalability challenges, there are presently two dominant lines of algorithmic workarounds. The first adopts various sampling techniques to extract much smaller computational subgraphs upon which GNN models can be trained in mini-batches. Examples include neighbor sampling [Hamilton et al., 2017, Ying et al., 2018], layer-wise sampling [Chen et al., 2018, Zou et al., 2019], and graph-wise sampling [Chiang et al., 2019, Zeng et al., 2021]. For each of these, there exist both online and offline versions, where the former involves randomly sampling new subgraphs during each training epoch, while the latter [Zeng et al., 2021, Gasteiger et al., 2022] is predicated on a fixed set of subgraphs for all epochs; MuseGNN will ultimately be based on a novel integration and analysis of this approach as will be introduced in Section 3.

The second line of work exploits the reuse of historical embeddings, meaning the embeddings of nodes computed and saved during the previous training epoch. In doing so, much of the recursive forward and backward computations required for GNN training, as well as expensive memory access to high-dimensional node features, can be reduced [Chen et al., 2017, Fey et al., 2021, Huang et al., 2023]. This technique has recently been applied to training unfolded GNN models [Xue et al., 2023], although available performance results do not cover large-scale graphs, there are no convergence guarantees, and no code is available (at least as of the time of this submission) for enabling further comparisons. Beyond this, we are unaware of prior work devoted to the scaling and coincident analysis of unfolded GNNs.

3 Graph-Regularized Energy Functions Infused with Sampling

Our goal of this section is to introduce a convenient family of energy functions formed by applying graph-based regularization to a set of subgraphs that have been sampled from a given graph of interest. For this purpose, we first present the offline sampling strategy which will undergird our approach, followed by details of energy functional form we construct on top of it for use with MuseGNN. Later, we conclude by analyzing special cases of these sampling-based energies, further elucidating relevant properties and connections with full-graph training.

3.1 Offline Sampling Foundation

In the present context, offline sampling refers to the case where we sample a fixed set of subgraphs from \mathcal{G} once and store them, which can ultimately be viewed as a form of preprocessing step. More formally, we assume an operator $\Omega : \mathcal{G} \rightarrow \{\mathcal{G}_s\}_{s=1}^m$, where $\mathcal{G}_s = \{\mathcal{V}_s, \mathcal{E}_s\}$ is a subgraph of \mathcal{G} containing $n_s = |\mathcal{V}_s|$ nodes, of which we assume n'_s are target training nodes (indexed from 1 to n'_s), and \mathcal{E}_s represents the edge set. The corresponding feature and label sets associated with the s -th subgraph are denoted $X_s \in \mathbb{R}^{n_s \times d}$ and $T_s \in \mathbb{R}^{n'_s \times d'}$, respectively.

There are several key reasons we employ offline sampling as the foundation for our scalable unfolded GNN architecture development. Firstly, conditioned on the availability of such pre-sampled/fixed subgraphs, there is no additional randomness when we use them to replace energy functions dependent on \mathcal{G} and X (e.g., as in (2)) with surrogates dependent on $\{\mathcal{G}_s, X_s\}_{s=1}^m$. Hence we retain a deterministic energy substructure contributing to a more transparent bilevel (upper- and lower-level) optimization process, as well as more interpretable node-wise embeddings that serve as attendant minimizers. Secondly, offline sampling allows us to conduct formal convergence analysis that is agnostic to the particular sampling operator Ω . In this

way, we need not compromise flexibility in choosing a practically-relevant Ω in order to maintain desirable convergence guarantees. For example, as will be detailed later, ShadowKHop [Zeng et al., 2021] sampling pairs well with our approach and directly adheres to our convergence analysis in Section 5. And lastly, offline sampling facilitates an attractive balance between model accuracy and efficiency within the confines of unfolded GNN architectures. As will be shown in Section 6, we can match the accuracy of full-graph training with an epoch time similar to online sampling methods, e.g., neighbor sampling.

3.2 Energy Function Formulation

To integrate offline sampling into a suitable graph-regularized energy function, we first introduce two sets of auxiliary variables that will serve as more flexible input arguments. Firstly, to accommodate multiple different embeddings for the same node appearing in multiple subgraphs, we define $Y_s \in \mathbb{R}^{n_s \times d}$ for each subgraph index $s = 1, \dots, m$, as well as $\mathbb{Y} = \{Y_s\}_{s=1}^m \in \mathbb{R}^{(\sum n_s) \times d}$ to describe the concatenated set. Secondly, we require additional latent variables that, as we will later see, facilitate a form of controllable linkage between the multiple embeddings that may exist for a given node (i.e., when a given node appears in multiple subgraphs). For this purpose, we define the latent variables as $M \in \mathbb{R}^{n \times d}$, where each row can be viewed as a shared summary embedding associated with each node in the original/full graph.

We then define our sampling-based extension of (2) for MuseGNN as

$$\ell_{\text{muse}}(\mathbb{Y}, M) := \sum_{s=1}^m \left[\|Y_s - f(X_s; W)\|_F^2 + \lambda \text{tr}(Y_s^\top L_s Y_s) + \gamma \|Y_s - \mu_s\|_F^2 + \sum_{i=1}^{n_s} \zeta(Y_{s,i}) \right], \quad (4)$$

where L_s is the graph Laplacian associated with \mathcal{G}_s , $\gamma \geq 0$ controls the weight of the additional penalty factor, and each $\mu_s \in \mathbb{R}^{n_s \times d}$ is derived from M as follows. Let $I(s, i)$ denote a function that maps the index of the i -th node in subgraph s to the corresponding node index in the full graph. For each subgraph s , we then define μ_s such that its i -th row satisfies $\mu_{s,i} = M_{I(s,i)}$; per this construction, $\mu_{s,i} = \mu_{s',j}$ if $I(s, i) = I(s', j)$. Consequently, $\{\mu_s\}_{s=1}^m$ and M represent the same overall set of latent embeddings, whereby the former is composed of repeated samples from the latter aligned with each subgraph.

Overall, there are three prominent factors which differentiate (4) from (2):

1. $\ell_{\text{muse}}(\mathbb{Y}, M)$ involves a deterministic summation over a fixed set of sampled subgraphs, where each Y_s is unique while W (and elements of M) are shared across subgraphs.
2. Unlike (2), the revised energy involves both an expanded set of node-wise embeddings \mathbb{Y} as well as auxiliary summary embeddings M . When later forming GNN layers designed to minimize $\ell_{\text{muse}}(\mathbb{Y}, M)$, we must efficiently optimize over *all* of these quantities, which alters the form of the final architecture.
3. The additional $\gamma \|Y_s - \mu_s\|_F^2$ penalty factor acts to enforce dependencies between the embeddings of a given node spread across different subgraphs.

With respect to the latter, it is elucidating to consider minimization of $\ell_{\text{muse}}(\mathbb{Y}, M)$ over \mathbb{Y} with M set to some fixed M' . In this case, up to an irrelevant global scaling factor and additive constant, the energy can be equivalently reexpressed as

$$\ell_{\text{muse}}(\mathbb{Y}, M = M') \equiv \sum_{s=1}^m \left[\|Y_s - [f'(X_s; W) + \gamma' \mu_s]\|_F^2 + \lambda' \text{tr}(Y_s^\top L_s Y_s) + \sum_{i=1}^{n_s} \zeta'(Y_{s,i}) \right], \quad (5)$$

where $f'(X_s; W) := \frac{1}{1+\gamma} f(X_s; W)$, $\gamma' := \frac{\gamma}{1+\gamma}$, $\lambda' := \frac{\lambda}{1+\gamma}$, and $\zeta'(Y_{s,i}) := \frac{1}{1+\gamma} \zeta(Y_{s,i})$. From this expression, we observe that, beyond inconsequential rescalings (which can be trivially neutralized by simply rescaling the original choices for $\{f, \gamma, \lambda, \zeta\}$), the role of μ_s is to refine the initial base predictor $f(X_s; W)$ with a corrective factor reflecting embedding summaries from other subgraphs sharing the same nodes. Conversely, when we minimize $\ell_{\text{muse}}(\mathbb{Y}, M)$ over M with \mathbb{Y} fixed, we find that the optimal μ_s for every s is equal to the *mean* embedding for each constituent node across all subgraphs. Hence M' chosen in this way via alternating minimization has a natural interpretation as grounding each Y_s to a shared average representation reflecting the full graph structure.

This reformulation provides additional entry points for interpretability as well. For example, if optimal solutions are such that Y_s and μ_s are similar while $f(X_s; W)$ is significantly different, we have a likely indication that, at least within this subgraph, graph structure and network effects are more dominant than node features. In contrast, if Y_s and $f(X_s; W)$ are similar with μ_s much less so, feature utility may be selectively strong for a given subgraph; however, if all three quantities are similar the situation is more indicative of strong overall node features. Beyond these considerations, we now consider two limiting special cases of $\ell_{\text{muse}}(\mathbb{Y}, M)$ that provide complementary contextualization.

3.3 Notable Limiting Cases

We first consider setting $\gamma = 0$, in which case the resulting energy completely decouples across each subgraph such that we can optimize each

$$\ell_{\text{muse}}^s(Y_s) := \|Y_s - f(X_s; W)\|_F^2 + \lambda \text{tr}(Y_s^\top L_s Y_s) + \sum_{i=1}^{n_s} \zeta(Y_{s,i}) \quad \forall s \quad (6)$$

independently. Under such conditions, the only cross-subgraph dependency stems from the shared base model weights W which are jointly trained. Hence $\ell_{\text{muse}}^s(Y_s)$ is analogous to a full graph energy as in (2) with \mathcal{G} replaced by \mathcal{G}_s . In Section 5 we will examine convergence conditions for the full bilevel optimization process over all Y_s and W that follows from the $\gamma = 0$ assumption. We have also found that this simplified setting performs well in practice; see Appendix B.1 for ablations.

At the opposite extreme when $\gamma = \infty$, we are effectively enforcing the constraint $Y_s = \mu_s$ for all s . As such, we can directly optimize all Y_s out of the model leading to the reduced M -dependent energy

$$\ell_{\text{muse}}(M) := \sum_{s=1}^m \left[\|\mu_s - f(X_s; W)\|_F^2 + \lambda \text{tr}(\mu_s^\top L_s \mu_s) + \sum_{i=1}^{n_s} \zeta(\mu_{s,i}) \right]. \quad (7)$$

Per the definition of $\{\mu_s\}_{s=1}^m$ and the correspondence with unique node-wise elements of M , this scenario has a much closer resemblance to full graph training with the original \mathcal{G} . In this regard, as long as a node from the original graph appears in at least one subgraph, then it will have a single, unique embedding in (7) aligned with a row of M .

Moreover, we can strengthen the correspondence with full-graph training via the suitable selection of the offline sampling operator Ω . In fact, there exists a simple uniform sampling procedure such that, at least in expectation, the energy from (7) is equivalent to the original full-graph version from (2), with the role of M equating to Y . More concretely, we present the following (all proofs are deferred to Appendix D):

Proposition 3.1. *Suppose we have m subgraphs $(\mathcal{V}_1, \mathcal{E}_1), \dots, (\mathcal{V}_m, \mathcal{E}_m)$ constructed independently such that $\forall s = 1, \dots, m, \forall u, v \in \mathcal{V}, \Pr[v \in \mathcal{V}_s] = \Pr[v \in \mathcal{V}_s \mid u \in \mathcal{V}_s] = p; (i, j) \in \mathcal{E}_s \iff i \in \mathcal{V}_s, j \in \mathcal{V}_s, (i, j) \in \mathcal{E}$. Then when $\gamma = \infty$, we have $\mathbb{E}[\ell_{\text{muse}}(M)] = mp \ell(M)$ with the λ in $\ell(M)$ rescaled to $p\lambda$.*

Strengthened by this result, we can more directly see that (7) provides an intuitive bridge between full-graph models based on (2) and subsequent subgraph models we intend to build via (4). Even so, we have found that relatively small γ values nonetheless work well in practice (although in principle it is actually possible to handle $\gamma = \infty$ using techniques like ADMM [Boyd et al., 2011]).

4 From Sampling-based Energies to the MuseGNN Framework

Having defined and motivated a family of sampling-based energy functions vis-a-vis (4), we now proceed to derive minimization steps that will serve as GNN model layers that define MuseGNN forward and backward passes as summarized in Algorithm 1. Given that there are two input arguments, namely \mathbb{Y} and M , it is natural to adopt an alternating minimization strategy whereby we fix one and optimize over the other, and vice versa.

With this in mind, we first consider optimization over \mathbb{Y} with M fixed. Per the discussion in Section 3.2, when conditioned on a fixed M , $\ell_{\text{muse}}(\mathbb{Y}, M)$ decouples over subgraphs. Consequently, optimization can proceed using subgraph-independent proximal gradient descent, leading to the update rule

$$Y_s^{(k)} = \text{prox}_\zeta \left[Y_s^{(k-1)} - \alpha \left([(1 + \gamma)I + \lambda L_s] Y_s^{(k-1)} - [f(X_s; W) + \gamma \mu_s] \right) \right], \quad \forall s. \quad (8)$$

Here the input argument to the proximal operator is given by a gradient step along (4) w.r.t. Y_s . We also remark that execution of (8) over K iterations represents the primary component of a single forward training pass of our proposed MuseGNN framework as depicted on lines 6-8 of Algorithm 1.

We next turn to optimization over M which, as mentioned previously, can be minimized by the mean of the subgraph-specific embeddings for each node. However, directly computing these means is problematic for computational reasons, as for a given node v this would require the infeasible collection of embeddings from all subgraphs containing v . Instead, we adopt an online mean estimator with forgetting factor ρ . For each node v in the full graph, we maintain a mean embedding M_v and a counter c_v . When this node appears in the s -th subgraph as node i (where i is the index within the subgraph), we update the mean embedding and counter via

$$M_{I(s,i)} \leftarrow \frac{\rho c_{I(s,i)}}{c_{I(s,i)} + 1} M_{I(s,i)} + \frac{(1 - \rho)c_{I(s,i)} + 1}{c_{I(s,i)} + 1} Y_{s,i}^{(K)}, \quad c_{I(s,i)} \leftarrow c_{I(s,i)} + 1. \quad (9)$$

Also shown on line 9 of Algorithm 1, we update M and c once per forward pass, which serves to refine the effective energy function observed by the core node embedding updates from (8).

For the backward pass, we compute gradients of

$$\mathcal{L}_{\text{muse}}(W, \theta) := \sum_{s=1}^m \sum_{i=1}^{n'_s} \mathcal{D} \left(g \left[Y_s^{(K)}(W)_i; \theta \right], T_{s,i} \right) \quad (10)$$

w.r.t. W and θ as listed on line 10 of Algorithm 1, where $\mathcal{L}_{\text{muse}}(W, \theta)$ is a sampling-based modification of (1). For W though, we only pass gradients through the calculation of $Y_s^{(K)}$, not the full online M update; however, provided ρ is chosen to be sufficiently large, M will change slowly relative to $Y_s^{(K)}$ such that this added complexity is not necessary for obtaining reasonable convergence.

Algorithm 1 Training procedure for MuseGNN

Input: $\{\mathcal{G}_s\}_{s=1}^m$: subgraphs, $\{X_s\}_{s=1}^m$: features, K : # unfolded layers, E : # epochs

- 1: Randomly initialize W and θ ; initialize $c \in \mathbb{R}^n$ and $M \in \mathbb{R}^{n \times d}$ to be zero
- 2: **for** $e = 1, 2, \dots, E$ **do**
- 3: **for** $s = 1, 2, \dots, m$ **do**
- 4: $\mu_{s,i} \leftarrow M_{I(s,i)}$, $i = 1, 2, \dots, n_s$
- 5: $Y_s^{(0)} \leftarrow f(X_s; W)$
- 6: **for** $k = 1, 2, \dots, K$ **do**
- 7: Update $Y_s^{(k)}$ from $Y_s^{(k-1)}$ by (8) using μ_s
- 8: **end for**
- 9: Update M and c using (9) with $Y_{s,i}^{(K)}$, $i = 1, 2, \dots, n_s$
- 10: Update W and θ via SGD over $\mathcal{L}_{\text{muse}}$ from (10)
- 11: **end for**
- 12: **end for**

5 Convergence Analysis of MuseGNN

Global Convergence with $\gamma = 0$. In the more restrictive setting where $\gamma = 0$, we derive conditions whereby the entire bilevel optimization pipeline converges to a solution that jointly minimizes both lower- and upper-level energy functions in a precise sense to be described shortly. We remark here that establishing convergence is generally harder for bilevel optimization problems relative to more mainstream, single-level alternatives [Colson et al., 2005]. To describe our main result, we first require the following definition:

Definition 5.1. Assume $f(X; W) = XW$, $\gamma = 0$, $\zeta(y) = 0$, $g(y; \theta) = y$, and that \mathcal{D} is a Lipschitz continuous convex function. Given the above, we then define $\mathcal{L}_{\text{muse}}^{(k)}(W)$ as (10) with K set to k . Analogously, we also define $\mathcal{L}_{\text{muse}}^*(W)$ as (10) with $Y_s^{(K)}$ replaced by $Y_s^* := \arg \min_{Y_s} \ell_{\text{muse}}^s(Y_s)$ for all s .

Theorem 5.2. Let W^* be the optimal value of the loss $\mathcal{L}_{\text{muse}}^*(W)$ per Definition 5.1, while $W^{(t)}$ denotes the value of W after t steps of stochastic gradient descent over $\mathcal{L}_{\text{muse}}^{(k)}(W)$ with diminishing step sizes $\eta_t = O(\frac{1}{\sqrt{t}})$. Then provided we choose $\alpha \in (0, \min_s \|I + \lambda L_s\|_2^{-1}]$ and $Y_s^{(0)} = f(X_s; W)$, for some constant C we have that

$$\mathbb{E} \left[\mathcal{L}_{\text{muse}}^{(k)}(W^{(t)}) \right] - \mathcal{L}_{\text{muse}}^*(W^*) \leq O \left(\frac{1}{\sqrt{t}} + e^{-Ck} \right).$$

Given that $\mathcal{L}_{\text{muse}}^*(W^*)$ is the global minimum of the combined bilevel system, this result guarantees that we can converge arbitrarily close to it with adequate upper- and lower-level iterations, i.e., t and k respectively. Note also that we have made no assumption on the sampling method. In fact, as long as offline sampling is used, convergence is guaranteed, although the particular offline sampling approach can potentially impact the convergence rate; see Appendix C.2 for further details.

Lower-Level Convergence with arbitrary γ . We now address the more general scenario where $\gamma \geq 0$ is arbitrary. However, because of the added challenge involved in accounting for alternating minimization over both \mathbb{Y} and M , it is only possible to establish conditions whereby the lower-level energy (4) is guaranteed to converge as follows.

Theorem 5.3. Assume $\zeta(y) = 0$. Suppose that we have a series of $\mathbb{Y}^{(k)}$ and $M^{(k)}$, $k = 0, 1, 2, \dots$ constructed following the updating rules $\mathbb{Y}^{(k)} := \arg \min_{\mathbb{Y}} \ell_{\text{muse}}(\mathbb{Y}, M^{(k-1)})$ and $M^{(k)} := \arg \min_M \ell_{\text{muse}}(\mathbb{Y}^{(k)}, M)$, with $\mathbb{Y}^{(0)}$ and $M^{(0)}$ initialized arbitrarily. Then

$$\lim_{k \rightarrow \infty} \ell_{\text{muse}}(\mathbb{Y}^{(k)}, M^{(k)}) = \inf_{\mathbb{Y}, M} \ell_{\text{muse}}(\mathbb{Y}, M). \quad (11)$$

While technically this result does not account for minimization over the upper-level MuseGNN loss, we still empirically find that the entire process outlined by Algorithm 1, including the online mean update, is nonetheless able to converge in practice. See Appendix C.1 for an illustration.

6 Experiments

We now seek to empirically show that MuseGNN serves as a reliable unfolded GNN model that:

1. Preserves competitive accuracy across datasets of widely varying size, including the very largest publicly-available graph benchmarks, with a single fixed architecture, and
2. Operates with comparable computational complexity relative to common alternatives that are also capable of scaling to the largest graphs.

For context though, we note that graph benchmark leaderboards often include top-performing entries based on complex compositions of existing models and training tricks, at times dependent on additional features or external data not included in the original designated dataset. Although these approaches have merit, our goal herein is not to compete with them, as they typically vary from dataset to dataset. Additionally, they are more frequently applied to smaller graphs using architectures that have yet to be consistently validated across multiple, truly large-scale benchmarks.

Datasets. We evaluate the performance of MuseGNN on node classification tasks from the Open Graph Benchmark (OGB) [Hu et al., 2020, 2021] and the Illinois Graph Benchmark (IGB) [Khatua et al., 2023]. Table 1 presents the details of these datasets, which are based on homogeneous graphs spanning a wide range of sizes. Of particular note is **IGB-full**, currently the largest publicly-available graph benchmark, along with a much smaller version called **IGB-tiny** that we include for comparison purposes. We also point out that while **MAG240M** is originally a heterogenous graph, we follow the common practice of homogenizing it [Hu et al., 2021]; similarly for IGB datasets, we adopt the provided homogeneous versions.

¹The size includes author and institution features.

Table 1: Dataset details, including node feature dimension (Dim.) and number of classes (# Class).

Dataset	$ \mathcal{V} $	$ \mathcal{E} $	Dim.	# Class	Dataset Size
ogbn-arxiv [Hu et al., 2020]	0.17M	1.2M	128	40	182MB
IGB-tiny [Khatua et al., 2023]	0.1M	0.5M	1024	19	400MB
ogbn-products [Hu et al., 2020]	2.4M	123M	100	47	1.4GB
ogbn-papers100M [Hu et al., 2020]	111M	1.6B	128	172	57GB
MAG240M [Hu et al., 2021]	244.2M	1.7B	768	153	377GB ¹
IGB-full [Khatua et al., 2023]	269.3M	4.0B	1024	19	1.15TB

MuseGNN Design. For *all* experiments, we choose the following fixed MuseGNN settings: Both $f(X; W)$ and $g(Y; \theta)$ are 3-layer MLPs, the number of unfolded layers K is 8 (rationale discussed later below), and the embedding dimension d is 512, and the forgetting factor ρ for the online mean estimation is 0.9. For offline subgraph sampling, we choose a variation on neighbor sampling called ShadowKHop [Zeng et al., 2021], which loosely approximates the conditions of Proposition 3.1. See Appendix A for further details regarding the MuseGNN implementation and hyperparameters.

Baseline Models. With the stated objectives of this section in mind, we compare MuseGNN with GCN [Kipf and Welling, 2017], GAT [Velickovic et al., 2018], and GraphSAGE [Hamilton et al., 2017], in each case testing with both neighbor sampling (NS) [Hamilton et al., 2017] and GNNAutoScale (GAS) [Fey et al., 2021] for scaling to large graphs. As a point of reference, we note that GAT with neighbor sampling is currently the top-performing homogeneous graph model on both the MAG240M and IGB-full leaderboards. We also compare with an analogous full-graph (FG) unfolded GNN (UGNN) with the same architecture as MuseGNN but without scalable sampling.

Accuracy Comparisons. As shown in Table 2, MuseGNN achieves similar accuracy to a comparable full-graph unfolded GNN model on the small datasets (satisfying our first objective from above), while the latter is incapable of scaling to even the mid-sized ogbn-products benchmark. Meanwhile, MuseGNN is generally better than the other GNN baselines, particularly so on the largest dataset, IGB-full. Notably, MuseGNN exceeds the performance of GAT with neighbor sampling, the current SOTA for homogeneous graph models on both MAG240M and IGB-full. Please also refer to Appendix B.1 for MuseGNN accuracy ablations involving γ , where we show that while even $\gamma = 0$ achieves strong results, increasing $\gamma > 0$ can lead to further improvement. Likewise, Appendix B.2 contains experiments showing that the improvement of MuseGNN is not merely a product of using ShadowKHop sampling instead of more traditional neighbor sampling with baseline models; there we show that when switched to offline ShadowKHop sampling, the baseline GNNs degrade further, possibly because they are not anchored to an integrated energy.

Timing Comparisons. Turning to model complexity, Table 3 displays the training speed of MuseGNN relative to two common baselines. From these results, we observe that MuseGNN executes with a similar epoch time (satisfying our second objective from above).

Convergence Illustration. In Figure 1 we show the empirical convergence of (4) w.r.t. \mathbb{Y} during the forward pass of MuseGNN models on ogbn-papers100M for differing values of γ . In all cases the energy converges within 8 iterations, supporting our choice of $K = 8$ for experiments.

7 Conclusion

In this work, we have proposed MuseGNN, an unfolded GNN model that scales to large datasets by incorporating offline graph sampling into the design of its lower-level, architecture-inducing energy function. In so doing, MuseGNN readily handles graphs with $\sim 10^8$ or more nodes and high-dimensional node features, exceeding 1TB in total size, all while maintaining interpretable layers with concomitant convergence guarantees.

Table 2: Node classification accuracy (%) on the test set, except for **MAG240M** which only has labels for validation set. Bold numbers denote the highest accuracy, and error bars are missing for some GNN baselines that were too expensive to compute. For the two largest datasets, MuseGNN is currently the top-performing homogeneous graph model on the relevant OGB-LSC and IGB leaderboards respectively, even while maintaining the interpretability attributes of an unfolded GNN. We omit error bars for baseline results in the two largest datasets because of the high cost to run them.

Model	Small		Medium	Large	Largest	
	arxiv	IGB-tiny	products	papers100M	MAG240M	IGB-full
GCN (NS)	69.71 \pm 0.25	69.77 \pm 0.11	78.49 \pm 0.53	65.83 \pm 0.36	65.24	48.59
SAGE (NS)	70.49 \pm 0.20	72.42 \pm 0.09	78.29 \pm 0.16	66.20 \pm 0.13	66.79	54.95
GAT (NS)	69.94 \pm 0.28	69.70 \pm 0.09	79.45 \pm 0.59	66.28 \pm 0.08	67.15	55.51
GCN (GAS)	71.68 \pm 0.3	67.86 \pm 0.20	76.6 \pm 0.3	54.2 \pm 0.7	OOM	OOM
SAGE (GAS)	71.35 \pm 0.4	69.35 \pm 0.06	77.7 \pm 0.7	57.9 \pm 0.4	OOM	OOM
GAT (GAS)	70.89 \pm 0.1	69.23 \pm 0.17	76.9 \pm 0.5	OOM	OOM	OOM
UGNN (FG)	72.74\pm0.25	72.44 \pm 0.09	OOM	OOM	OOM	OOM
MuseGNN	72.50 \pm 0.19	72.80\pm0.02	80.47\pm0.16	66.82\pm0.02	67.26\pm0.06	60.21\pm0.18

Table 3: Training speed (epoch time) in seconds; hardware configurations in Appendix A. Even on the largest graph, **IGB-full**, MuseGNN remains comparable to popular baselines that adopt online sampling.

Model	papers-100M	MAG240M	IGB-full
SAGE (NS)	102.48	795.19	17279.98
GAT (NS)	164.14	1111.30	19789.79
MuseGNN	158.85	1370.47	20413.69

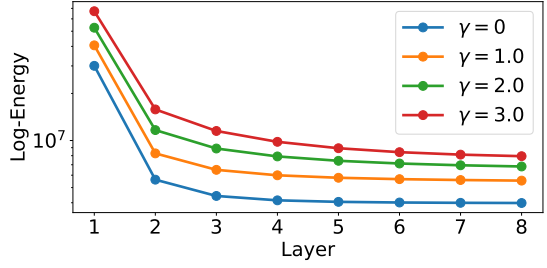


Figure 1: Convergence of (4) for MuseGNN trained on **papers100M** with varying γ .

References

Hongjoon Ahn, Yongyi Yang, Quan Gan, Taesup Moon, and David P Wipf. Descent steps of a relation-aware energy produce heterogeneous graph neural networks. *Advances in Neural Information Processing Systems*, 35:38436–38448, 2022.

Stephen Boyd, Neal Parikh, Eric Chu, Borja Peleato, Jonathan Eckstein, et al. Distributed optimization and statistical learning via the alternating direction method of multipliers. *Foundations and Trends® in Machine learning*, 3(1):1–122, 2011.

Sébastien Bubeck et al. Convex optimization: Algorithms and complexity. *Foundations and Trends® in Machine Learning*, 8(3-4):231–357, 2015.

Jianfei Chen, Jun Zhu, and Le Song. Stochastic training of graph convolutional networks with variance reduction. *arXiv preprint arXiv:1710.10568*, 2017.

Jie Chen, Tengfei Ma, and Cao Xiao. FastGCN: fast learning with graph convolutional networks via importance sampling. *arXiv preprint arXiv:1801.10247*, 2018.

Jiuhai Chen, Jonas Mueller, Vassilis N. Ioannidis, Soji Adeshina, Yangkun Wang, Tom Goldstein, and David Wipf. Does your graph need a confidence boost? convergent boosted smoothing on graphs with tabular node features. In *International Conference on Learning Representations*, 2022. URL <https://openreview.net/forum?id=nHpzE7DqAnG>.

Siheng Chen and Yonina C Eldar. Graph signal denoising via unrolling networks. In *ICASSP 2021-2021 IEEE International Conference on Acoustics, Speech and Signal Processing (ICASSP)*, pages 5290–5294, 2021.

Wei-Lin Chiang, Xuanqing Liu, Si Si, Yang Li, Samy Bengio, and Cho-Jui Hsieh. Cluster-GCN: An efficient algorithm for training deep and large graph convolutional networks. In *Proceedings of the 25th ACM SIGKDD international conference on knowledge discovery & data mining*, pages 257–266, 2019.

Benoît Colson, Patrice Marcotte, and Gilles Savard. Bilevel programming: A survey. *4or*, 3:87–107, 2005.

Patrick L Combettes and Jean-Christophe Pesquet. Proximal splitting methods in signal processing. *Fixed-point algorithms for inverse problems in science and engineering*, pages 185–212, 2011.

I. Csiszár and G. Tusnády. Information geometry and alternating minimization procedures. *Statistics and Decisions*, Supplemental Issue Number 1:205–237, 1984.

Francesco Di Giovanni, James Rowbottom, Benjamin Paul Chamberlain, Thomas Markovich, and Michael M Bronstein. Understanding convolution on graphs via energies. *Transactions on Machine Learning Research*, 2023.

Matthias Fey, Jan E Lenssen, Frank Weichert, and Jure Leskovec. GNNAutoScale: Scalable and expressive graph neural networks via historical embeddings. In *International Conference on Machine Learning*, pages 3294–3304. PMLR, 2021.

Johannes Gasteiger, Aleksandar Bojchevski, and Stephan Günnemann. Predict then propagate: Graph neural networks meet personalized pagerank. In *International Conference on Learning Representations*, 2019. URL <https://openreview.net/forum?id=H1gL-2A9Ym>.

Johannes Gasteiger, Chendi Qian, and Stephan Günnemann. Influence-based mini-batching for graph neural networks. In *Learning on Graphs Conference*, pages 9–1. PMLR, 2022.

Justin Gilmer, Samuel S Schoenholz, Patrick F Riley, Oriol Vinyals, and George E Dahl. Neural message passing for quantum chemistry. In *International Conference on Machine Learning*, pages 1263–1272. PMLR, 2017.

Fangda Gu, Heng Chang, Wenwu Zhu, Somayeh Sojoudi, and Laurent El Ghaoui. Implicit graph neural networks. In *Advances in Neural Information Processing Systems*, 2020.

Will Hamilton, Zhitao Ying, and Jure Leskovec. Inductive representation learning on large graphs. *Advances in Neural Information Processing Systems*, 30, 2017.

Weihua Hu, Matthias Fey, Marinka Zitnik, Yuxiao Dong, Hongyu Ren, Bowen Liu, Michele Catasta, and Jure Leskovec. Open graph benchmark: Datasets for machine learning on graphs. *Advances in Neural Information Processing Systems*, 33:22118–22133, 2020.

Weihua Hu, Matthias Fey, Hongyu Ren, Maho Nakata, Yuxiao Dong, and Jure Leskovec. OGB-LSC: A large-scale challenge for machine learning on graphs. *arXiv:2103.09430*, 2021.

Kezhao Huang, Haitian Jiang, Minjie Wang, Guangxuan Xiao, David Wipf, Xiang Song, Quan Gan, Zengfeng Huang, Jidong Zhai, and Zheng Zhang. Refresh: Reducing memory access from exploiting stable historical embeddings for graph neural network training. *arXiv preprint arXiv:2301.07482*, 2023.

Steven M. Kearnes, Kevin McCloskey, Marc Berndl, Vijay S. Pande, and Patrick Riley. Molecular graph convolutions: moving beyond fingerprints. *J. Comput. Aided Mol. Des.*, 30(8):595–608, 2016.

Arpandeep Khatua, Vikram Sharma Mailthody, Bhagyashree Taleka, Tengfei Ma, Xiang Song, and Wen-mei Hwu. Igb: Addressing the gaps in labeling, features, heterogeneity, and size of public graph datasets for deep learning research. *arXiv preprint arXiv:2302.13522*, 2023.

Diederik P Kingma and Jimmy Ba. Adam: A method for stochastic optimization. *arXiv preprint arXiv:1412.6980*, 2014.

Thomas N. Kipf and Max Welling. Semi-Supervised Classification with Graph Convolutional Networks. In *Proceedings of the 5th International Conference on Learning Representations, ICLR '17*, Palais des Congrès Neptune, Toulon, France, 2017. URL <https://openreview.net/forum?id=SU4ayYg1>.

Qimai Li, Zhichao Han, and Xiao-Ming Wu. Deeper insights into graph convolutional networks for semi-supervised learning. In *Proceedings of the AAAI Conference on Artificial Intelligence*, volume 32, 2018.

Yao Ma, Xiaorui Liu, Tong Zhao, Yozen Liu, Jiliang Tang, and Neil Shah. A unified view on graph neural networks as graph signal denoising. In *Proceedings of the 30th ACM International Conference on Information & Knowledge Management*, pages 1202–1211, 2021.

Arkadi Nemirovski, Anatoli Juditsky, Guanghui Lan, and Alexander Shapiro. Robust stochastic approximation approach to stochastic programming. *SIAM Journal on optimization*, 19(4):1574–1609, 2009.

Kenta Oono and Taiji Suzuki. Graph neural networks exponentially lose expressive power for node classification. In *8th International Conference on Learning Representations, ICLR*, 2020.

Xuran Pan, Shiji Song, and Gao Huang. A unified framework for convolution-based graph neural networks. *arXiv preprint arXiv:2107.10234*, 2020.

Adam Paszke, Sam Gross, Francisco Massa, Adam Lerer, James Bradbury, Gregory Chanan, Trevor Killeen, Zeming Lin, Natalia Gimelshein, Luca Antiga, et al. Pytorch: An imperative style, high-performance deep learning library. *Advances in Neural Information Processing Systems*, 32, 2019.

Ke Sun, Zhanxing Zhu, and Zhouchen Lin. AdaGCN: AdaBoosting graph convolutional networks into deep models. *arXiv preprint arXiv:1908.05081*, 2019.

Petar Velickovic, Guillem Cucurull, Arantxa Casanova, Adriana Romero, Pietro Liò, and Yoshua Bengio. Graph attention networks. In *6th International Conference on Learning Representations, ICLR 2018, Vancouver, BC, Canada, April 30 - May 3, 2018, Conference Track Proceedings*, Vancouver, BC, Canada, 2018. OpenReview.net. URL <https://openreview.net/forum?id=rJXMpikCZ>.

Minjie Yu Wang. Deep graph library: Towards efficient and scalable deep learning on graphs. In *ICLR workshop on representation learning on graphs and manifolds*, 2019.

Rui Xue, Haoyu Han, MohamadAli Torkamani, Jian Pei, and Xiaorui Liu. Lazygnn: Large-scale graph neural networks via lazy propagation. *arXiv preprint arXiv:2302.01503*, 2023.

Yongyi Yang, Tang Liu, Yangkun Wang, Jinjing Zhou, Quan Gan, Zhewei Wei, Zheng Zhang, Zengfeng Huang, and David Wipf. Graph neural networks inspired by classical iterative algorithms. In *International Conference on Machine Learning*, pages 11773–11783. PMLR, 2021.

Yongyi Yang, Tang Liu, Yangkun Wang, Zengfeng Huang, and David Wipf. Implicit vs unfolded graph neural networks. *arXiv preprint arXiv:2111.06592*, 2022.

Rex Ying, Ruining He, Kaifeng Chen, Pong Eksombatchai, William L Hamilton, and Jure Leskovec. Graph convolutional neural networks for web-scale recommender systems. In *Proceedings of the 24th ACM SIGKDD international conference on knowledge discovery & data mining*, pages 974–983, 2018.

Zhitao Ying, Dylan Bourgeois, Jiaxuan You, Marinka Zitnik, and Jure Leskovec. Gnnexplainer: Generating explanations for graph neural networks. *Advances in neural information processing systems*, 32, 2019.

Hanqing Zeng, Muhan Zhang, Yinglong Xia, Ajitesh Srivastava, Andrey Malevich, Rajgopal Kannan, Viktor Prasanna, Long Jin, and Ren Chen. Decoupling the depth and scope of graph neural networks. *Advances in Neural Information Processing Systems*, 34, 2021.

Hongwei Zhang, Tijin Yan, Zenjun Xie, Yuanqing Xia, and Yuan Zhang. Revisiting graph convolutional network on semi-supervised node classification from an optimization perspective. *arXiv preprint arXiv:2009.11469*, 2020.

Dengyong Zhou, Olivier Bousquet, Thomas Lal, Jason Weston, and Bernhard Schölkopf. Learning with local and global consistency. *Advances in neural information processing systems*, 16, 2003.

Meiqi Zhu, Xiao Wang, Chuan Shi, Houye Ji, and Peng Cui. Interpreting and unifying graph neural networks with an optimization framework. In *Proceedings of the Web Conference 2021*, pages 1215–1226, 2021.

Difan Zou, Ziniu Hu, Yewen Wang, Song Jiang, Yizhou Sun, and Quanquan Gu. Layer-dependent importance sampling for training deep and large graph convolutional networks. *Advances in Neural Information Processing Systems*, 32, 2019.

A Experiment Details

Model Details. For MuseGNN, we choose the base model $f(X; W)$ and output function $g(Y; \theta)$ to be two shallow 3-layer MLPs with standard residual skip connections (although for the somewhat differently-structured `ogbn-products` data we found that skip connections were not necessary). The number of unfolded layers, K , is selected to be 8, and the hidden dimension d is set to 512. The forgetting factor ρ for the online mean estimation is set to be 0.9. All the models and experiments are implemented in PyTorch [Paszke et al., 2019] using the Deep Graph Library (DGL) [Wang, 2019].

Offline Samples. As supported by Proposition 3.1, subgraphs induced from nodes (where all the edges between sampled nodes are kept) pair naturally with the energy function. Therefore we use node-induced subgraphs for our experiments. For `ogbn-arxiv`, we use the 2-hop full neighbor because it is a relatively small graph. For `IGB-tiny`, `ogbn-papers100M`, and `MAG240M`, we use ShadowKHop with fanout [5,10,15]. For the rest of the datasets, we use ShadowKHop with fanout [10, 15]. Note that ShadowKHop sampler performs node-wise neighbor sampling and returns the subgraph induced by all the sampled nodes.

Training Hyperparameters. In the training process, we set the dropout rate of the MLP layers to be 0.2, and we do not have dropout between the propagation layers. The parameters are optimized by Adam optimizer [Kingma and Ba, 2014] with the weight decay parameter set to 0 and the learning rate being 0.001. For `ogbn-arxiv` and `ogbn-papers100M`, $\alpha = 0.05, \lambda = 20$. For `MAG240M` and the `IGB` series datasets, $\alpha = 0.2, \lambda = 4$. And for `ogbn-products`, $\alpha = \lambda = 1$ with preconditioning on the degree matrix for each unfolded step/layer. The batch size n'_s in the offline samples are all set to 1000. For large-scale datasets, an expensive hyperparameter grid search as commonly used for GNN tuning is not feasible. Hence we merely applied simple heuristics informed from training smaller models to pick hyperparameters for the larger datasets. Also it is worth noticing that α should not in principle affect accuracy if set small enough, since the model will eventually converge. In this regard, α can be set dependent on λ , since the latter determines the size of α needed for convergence.

Evaluation Process. In the presented results, the evaluation process for validation and test datasets uses the same pipeline as the training process does: doing offline sampling first and then use these fixed samples to do the calculation. The only difference is that in the evaluation process, the backward propagation is not performed. While we used the same pipeline for training and testing, MuseGNN is modular and we could optionally use online sampling for the evaluation or even multi-hop full-neighbor loader in the evaluation time.

Configurations in the Speed Experiments. We use a single AWS EC2 p4d.24xlarge instance to run the speed experiments. It comes with dual Intel Xeon Platinum 8275CL CPU (48 cores, 96 threads), 1.1TB main memory and 8 A100 (40GB) GPUs. All the experiments are run on single GPU. When running MuseGNN, the pre-sampled graph structures are stored in the NVMe SSDs and the input feature is loaded into the main memory (for `IGB-full`, its feature exceeds the capacity of the main memory, so mmap is employed). In the baseline setting, `ogbn-papers100M` and `MAG240M` are paired with neighbor sampling of fanout [5, 10, 15] and `IGB-full` is paired with neighbor sampling of fanout [10, 15]. So the fanout for the online neighbor sampling baselines and MuseGNN are the same so that they can have a fair comparison. In these experiments, the hidden size is set to 256 as commonly does.

Model Code. Because ICLR submissions are public, we choose not to release the code until the decision.

B Addtional Experiments and Discussions

B.1 Further Details Regarding the Role of γ in MuseGNN

The incorporation of $\gamma > 0$ serves two purposes within our MuseGNN framework and its supporting analysis. First, by varying γ we are able to build a conceptual bridge between the decoupled/inductive $\gamma = 0$ base

scenario, and full-graph training as $\gamma \rightarrow \infty$, provided the sampled subgraphs adhere to the conditions of Proposition 3.1. In this way, the generality of $\gamma > 0$ has value in terms of elucidating connections between modeling regimes, independently of empirical performance.

That being said, the second role is more pragmatic, as $\gamma > 0$ can indeed improve predictive accuracy. As shown in the ablation in Table 4 (where all hyperparameters except γ remain fixed), $\gamma = 0$ already achieves good performance; however, increasing γ leads to further improvements. This is likely because larger γ enables the model to learn similar embeddings for the same node in different subgraphs, which may be more robust to the sampling process.

Table 4: Ablation study of the penalty factor γ . Results shown represent the accuracy (%) on the test set. Bold numbers denote the best performing method.

	$\gamma = 0$	$\gamma = 0.1$	$\gamma = 0.5$	$\gamma = 1$	$\gamma = 2$	$\gamma = 3$
<code>papers100M</code>	66.29	66.31	66.53	66.45	66.64	66.82

That being said, while we can improve accuracy with $\gamma > 0$, this generality comes with an additional memory cost for storing the required mean vectors. However, this memory complexity for the mean vectors is only $O(nd)$, which is preferable to the memory complexity $O(ndK)$ of GAS [Fey et al., 2021], which depends on the number of layers K . Importantly, this more modest $O(nd)$ storage is only an upper bound for the MuseGNN memory complexity, as the $\gamma = 0$ case is already very effective even without requiring additional storage. As an additional point of reference, the GAS-related approach from [Xue et al., 2023] also operates with only single-layer $O(nd)$ of additional storage; however, unlike MuseGNN, this storage is mandatory for large graphs (not amenable to full-graph training) and therefore serves as a *lower* bound for memory complexity. Even so, the approach from [Xue et al., 2023] is valuable and complementary, and should their code become available in the future, it would be interesting to explore the possibility of integrating with MuseGNN.

B.2 Sampling Ablation on the Baseline Models

We choose neighbor sampling for the baselines because it is most commonly used, but since ShadowKHop is paired with MuseGNN, we use Table 5 to show that the improvement is not coming from the change in the sampling method but the usage of energy-based scalable unfolded model. In Table 5, the baseline models are trained on `ogbn-papers100M` with the same offline ShadowKHop samples used in the training of MuseGNN, but they suffer from a decrease in the accuracy compared with the online neighbor sampling counterparts, so the change in sampling method cannot account for the enhancement in the accuracy.

Table 5: Ablation study of the accuracy improvement compared with baselines. Shown results are the accuracy (%) on the test set of `ogbn-papers100M`.

Baseline Model			
Sampling Method	GCN	GAT	SAGE
ShadowKHop (offline)	64.89	63.84	65.57
Neighbor Sampling (online)	65.83	66.28	66.2

B.3 Alternative Sampling Method for MuseGNN

We also paired MuseGNN with online neighbor sampling, the most popular choice for sampling, on `ogbn-papers100M` to account for our design choice of sampling methods coupled with MuseGNN. Theoretically, the convergence guarantee no longer holds true for online sampling. Additionally, neighbor sampling removes terms regarding edge information from the energy function, so we expect it to be worse than the offline ShadowKHop sampling that we use. This is also supported by Proposition 3.1 because neighbor sampling does not provide

subgraphs induced from the nodes with all the edges. Empirically, with online neighbor sampling, the test accuracy is 66.11%; it is indeed lower than the 66.82% from our offline ShadowKHop results.

C Additional Convergence Details

C.1 Empirical Convergence Results

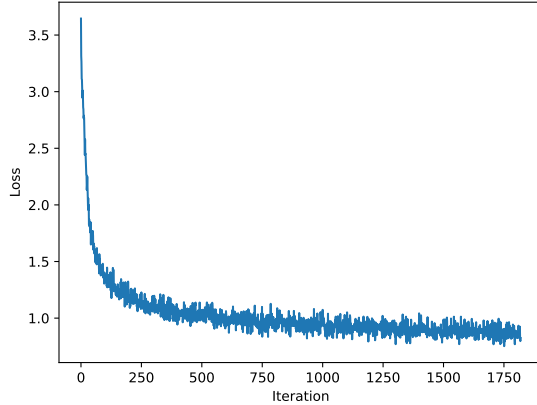


Figure 2: Convergence of the upper-level loss on `ogbn-arxiv` dataset for 20 epochs with penalty factor $\gamma = 1$.

C.2 A Note on Sampling Methods Impacting Convergence Rates

As stated in the main paper, offline sampling allows us to conduct formal convergence analysis that is agnostic to the particular sampling operator. So our convergence guarantee is valid for all sampling methods. However, different sampling methods can still actually have an impact on the convergence *rate* of the bilevel optimization. This is because different sampling methods will produce subgraphs with different graph Laplacian matrices, and the latter may have differing condition numbers $\frac{\sigma}{\tau}$ as mentioned later in Lemma D.4. In this regard, a larger such condition number will generally yield a slower convergence rate. Further details are elaborated in the proof of Theorem 5.2 in Appendix D.2.

D Proofs

D.1 Connection with Full Graph Training

Proposition 3.1. *Suppose we have m subgraphs $(\mathcal{V}_1, \mathcal{E}_1), \dots, (\mathcal{V}_m, \mathcal{E}_m)$ constructed independently such that $\forall s = 1, \dots, m, \forall u, v \in \mathcal{V}, \Pr[v \in \mathcal{V}_s] = \Pr[v \in \mathcal{V}_s \mid u \in \mathcal{V}_s] = p; (i, j) \in \mathcal{E}_s \iff i \in \mathcal{V}_s, j \in \mathcal{V}_s, (i, j) \in \mathcal{E}$. Then when $\gamma = \infty$, we have $\mathbb{E}[\ell_{muse}(M)] = mp \ell(M)$ with the λ in $\ell(M)$ rescaled to $p\lambda$.*

Proof. The probability that an edge is sampled is $\Pr[(i, j) \in \mathcal{E}_s \mid (i, j) \in \mathcal{E}] = p^2$. $\forall v \in \mathcal{V}$, if $v \in \mathcal{V}_s, v \in \mathcal{V}_t$,

then $Y_{s,v} = Y_{t,v} = M_v$. We have

$$\begin{aligned}
\ell_{\text{muse}}(M) &= \sum_{s=1}^m \left[\sum_{v \in \mathcal{V}_s} \left(\|M_v - f(X; W)_v\|_2^2 + \zeta(M_v) \right) + \frac{\lambda}{2} \sum_{(i,j) \in \mathcal{E}_s} \|M_i - M_j\|_2^2 \right] \\
\mathbb{E} [\ell_{\text{muse}}(M)] &= \sum_{s=1}^m \sum_{v \in \mathcal{V}_s} \left(\|M_v - f(X; W)_v\|_2^2 + \zeta(M_v) \right) \cdot \Pr[v \in \mathcal{V}_s] \\
&\quad + \frac{\lambda}{2} \sum_{s=1}^m \sum_{(i,j) \in \mathcal{E}_s} \|M_i - M_j\|_2^2 \cdot \Pr[(i,j) \in \mathcal{E}_s] \\
&= mp \sum_{v \in \mathcal{V}} \left(\|M_v - f(X; W)_v\|_2^2 + \zeta(M_v) \right) + mp^2 \frac{\lambda}{2} \sum_{(i,j) \in \mathcal{E}} \|M_i - M_j\|_2^2 \\
&= mp \left[\|M - f(X; W)\|_F^2 + p\lambda \text{tr}(M^\top LM) + \sum_{i=1}^n \zeta(M_i) \right] \\
&= mp \ell(M)
\end{aligned}$$

□

D.2 Full Convergence Analysis

According to Definition 5.1, $Y_s^*(W) = (I + \lambda L_s)^{-1} f(X_s; W) := P_s^* f(X_s; W)$ is the optimal embedding for the subgraph energy $\ell_{\text{muse}}^s(Y_s)$. Additionally, we initialize $Y_s^{(0)}$ as $f(X_s; W)$, so $Y_s^{(k)}$ can be written as $P_s^{(k)} f(X; W)$ where $P_s^{(k)}$ is also a matrix. We have $\alpha \leq \|I + \lambda L_s\|_2^{-1}$, so $P_s^{(k)}$ will converge to P_s^* as k grows. The output of \mathcal{D} over matrix input is the sum of \mathcal{D} over each row vectors, as typical discriminator function like squared error or cross-entropy do.

Plugging the $Y_s^{(k)}(W)$ and $Y_s^*(W)$ into the loss function, we have

$$\mathcal{L}_{\text{muse}}^{(k)}(W) = \sum_{s=1}^m \mathcal{D} \left(Y_s^{(k)}(W)_{1:n'_s}, T_s \right) = \mathcal{D} \left(\mathbb{P}^{(k)} \mathbb{X} W, \mathbb{T} \right) \quad (12)$$

where $1 : n'_s$ means the first n'_s rows, $\mathbb{T} := (T_1, T_2, \dots, T_m)^\top$, $\mathbb{P}^{(k)} := \text{diag} \left\{ \left(P_s^{(k)} \right)_{1:n'_s} \right\}_{s=1}^m$. Similarly, for $\ell_W^*(W)$, we change all the $Y_s^{(k)}$ and $P_s^{(k)}$ to Y_s^* and P_s^* . That is,

$$\mathbb{P}^* := \text{diag} \left\{ \left(P_s^* \right)_{1:n'_s} \right\}_{s=1}^m, \quad \mathcal{L}_{\text{muse}}^*(W) = \mathcal{D} \left(\mathbb{P}^* \mathbb{X} W, \mathbb{T} \right)$$

Stochastic Gradient Descent The updating rule by gradient descent for the parameter is

$$W^{(t+1)} = W^{(t)} - \eta \nabla_{W^{(t)}} \mathcal{L}_{\text{muse}}^{(k)}(W^{(t)}) = W^{(t)} - \eta \sum_{s=1}^m \frac{\partial \mathcal{D} \left(Y_s^{(k)}(W^{(t)}), T_s \right)}{\partial W^{(t)}}$$

In reality, we use stochastic gradient descent to minimize $\mathcal{L}_{\text{muse}}^{(k)}(W)$, and the updating rule becomes

$$W^{(t+1)} = W^{(t)} - \eta \frac{\partial \mathcal{D} \left(T_s, g \left(Y_s^{(k)}(W^{(t)}) \right) \right)}{\partial W^{(t)}} \quad (13)$$

Here s is picked at random from $\{1, 2, \dots, m\}$, so the gradient is an unbiased estimator of the true gradient.

Lemma D.1. *As defined in (12), $\mathcal{L}_{\text{muse}}^{(k)}(W)$ is a convex function of W . Furthermore, there exist the global optimal $W^{(k*)}$ such that $\mathcal{L}_{\text{muse}}^{(k)}(W^{(k*)}) \leq \mathcal{L}_{\text{muse}}^{(k)}(W)$ for all W .*

Proof. $\mathcal{L}_{\text{muse}}^{(k)}(W)$ is a composition of convex function \mathcal{D} with an affine function, so the convexity is retained. By the convexity, the global optimal $W^{(k*)}$ exists. \square

Lemma D.2. *When the loss function $\mathcal{L}_{\text{muse}}^{(k)}$ is defined as equation (12), and the parameter W is updated by (13) with diminishing step sizes $\eta_t = O(\frac{1}{\sqrt{t}})$, $\mathbb{E} \left[\mathcal{L}_{\text{muse}}^{(k)}(W^{(t)}) \right] - \mathcal{L}_{\text{muse}}^{(k)}(W^{(k*)}) = O(1/\sqrt{t})$.*

Proof. Since the loss function $\mathcal{L}_{\text{muse}}^{(k)}$ is convex by Lemma D.1, and the step size is diminishing in $O(\frac{1}{\sqrt{t}})$, by Nemirovski et al. [2009], the convergence rate of the difference in expected function value and optimal function value is $O(\frac{1}{\sqrt{t}})$. \square

Lemma D.3. *The subgraph energy function (6) with $\zeta(y) = 0$ (as defined in Definition 5.1) is σ_s -smooth and τ_s -strongly convex with respect to Y_s , with $\sigma_s = \sigma_{\max}(I + \lambda L_s)$ and $\tau_s = \sigma_{\min}(I + \lambda L_s)$, where σ_{\max} and σ_{\min} are the maximum and minimum singular value of the matrix.*

Proof. The proof is simple by computing the Hessian of the energy function. Additionally, since the graph Laplacian matrix L_s is positive-semidefinite, we have $\sigma_s \geq \tau_s > 0$. \square

Lemma D.4. *Let $\sigma, \tau = \arg \max_{\sigma_s, \tau_s} \frac{\sigma_s}{\tau_s}, s = 1, 2, \dots, m$, where $\frac{\sigma}{\tau}$ gives the worst condition number of all subgraph energy functions. In the descent iterations from (8) that minimizes (6) with step size $\alpha = \frac{1}{\sigma}$, we can establish the bound on the propagation matrix $\|\mathbb{P}^{(k)} - \mathbb{P}^*\| \leq m \exp(-\frac{\tau}{2\sigma}k) \sum_{s=1}^m \|P_s^{(0)} - P_s^*\|$*

Proof. By Bubeck et al. [2015][Theorem 3.10], we have

$$\left\| P_s^{(k)} f(X; W) - P_s^* f(X; W) \right\|^2 \leq e^{-\frac{\tau_s}{\sigma_s} k} \left\| P_s^{(0)} f(X; W) - P_s^* f(X; W) \right\|^2$$

Since this bound holds true for any $f(X; W)$, by choosing $f(X; W) = I$ to be the identity matrix, we have

$$\left\| P_s^{(k)} - P_s^* \right\| \leq e^{-\frac{\tau_s}{2\sigma_s} k} \left\| P_s^{(0)} - P_s^* \right\| \leq e^{-\frac{\tau}{2\sigma} k} \left\| P_s^{(0)} - P_s^* \right\|$$

Adding up all the m subgraphs, we have

$$\left\| \mathbb{P}^{(k)} - \mathbb{P}^* \right\| \leq m e^{-\frac{\tau}{2\sigma} k} \sum_{s=1}^m \left\| P_s^{(0)} - P_s^* \right\|$$

\square

Theorem 5.2. *Let W^* be the optimal value of the loss $\mathcal{L}_{\text{muse}}^*(W)$ per Definition 5.1, while $W^{(t)}$ denotes the value of W after t steps of stochastic gradient descent over $\mathcal{L}_{\text{muse}}^{(k)}(W)$ with diminishing step sizes $\eta_t = O(\frac{1}{\sqrt{t}})$. Then provided we choose $\alpha \in (0, \min_s \|I + \lambda L_s\|_2^{-1}]$ and $Y_s^{(0)} = f(X_s; W)$, for some constant C we have that*

$$\mathbb{E} \left[\mathcal{L}_{\text{muse}}^{(k)}(W^{(t)}) \right] - \mathcal{L}_{\text{muse}}^*(W^*) \leq O \left(\frac{1}{\sqrt{t}} + e^{-Ck} \right).$$

Proof. In Definition 5.1, we assume \mathcal{D} to be Lipschitz continuous for the embedding variable, so for any input \mathbb{Y} and \mathbb{Y}' , we have $|\mathcal{D}(\mathbb{Y}, \mathbb{T}) - \mathcal{D}(\mathbb{Y}', \mathbb{T})| \leq L_{\mathcal{D}} \|\mathbb{Y} - \mathbb{Y}'\|$.

$$\begin{aligned} & \mathcal{L}_{\text{muse}}^{(k)}(W^{(k*)}) - \mathcal{L}_{\text{muse}}^*(W^*) \\ & \leq \mathcal{L}_{\text{muse}}^{(k)}(W^*) - \mathcal{L}_{\text{muse}}^*(W^*) \\ & = \mathcal{D}(\mathbb{P}^{(k)} \mathbb{X} W^*, \mathbb{T}) - \mathcal{D}(\mathbb{P}^* \mathbb{X} W^*, \mathbb{T}) \\ & \leq L_{\mathcal{D}} \left\| \mathbb{P}^{(k)} \mathbb{X} W^* - \mathbb{P}^* \mathbb{X} W^* \right\| \\ & \leq L_{\mathcal{D}} \left\| \mathbb{P}^{(k)} - \mathbb{P}^* \right\| \|\mathbb{X} W^*\| \\ & \leq O \left(e^{-\frac{\tau}{2\sigma} k} \right) \end{aligned}$$

Therefore,

$$\begin{aligned}
& \mathbb{E} \left[\mathcal{L}_{\text{muse}}^{(k)}(W^{(t)}) \right] - \mathcal{L}_{\text{muse}}^*(W^*) \\
&= \mathbb{E} \left[\mathcal{L}_{\text{muse}}^{(k)}(W^{(t)}) \right] - \mathcal{L}_{\text{muse}}^{(k)}(W^{(k*)}) + \mathcal{L}_{\text{muse}}^{(k)}(W^{(k*)}) - \mathcal{L}_{\text{muse}}^*(W^*) \\
&\leq O\left(\frac{1}{\sqrt{t}}\right) + O(e^{-\frac{\tau}{2\sigma}k}) \\
&\leq O\left(\frac{1}{\sqrt{t}} + e^{-ck}\right)
\end{aligned}$$

where $c = \frac{\tau}{2\sigma}$. \square

D.3 Alternating Minimization

The main reference for alternating minimization is Csiszár and Tusnády [1984]. In this paper, they proved that the alternating minimization method will converge to the optimal value when a five-point property or both a three-point property and a four-point property holds true. We will show that the global energy function and the corresponding updating rule satisfy the three-point property and the four-point property. Thus, the alternating minimization method will converge to the optimal value.

For simplicity, we define $r_{s,i}$ as $r_{s,i} = \sum_{s'=1}^m \sum_{j=1}^{n'_s} \mathbb{I}\{I(s,i) = I(s',j)\}$, where $\mathbb{I}\{\cdot\}$ is the indicator function. Therefore, $r_{s,i}$ means the node in the full graph with index $I(s,i)$ appears $r_{s,i}$ times in all subgraphs. With some abuse of the notation, we let $r_{I(s,i)} = r_{s,i}$.

In the energy function (4), we still want to find a set of $\{Y_s\}_{s=1}^m$ and $\{\mu_s\}_{s=1}^m$ to minimize the global energy function. We can use the alternating minimization method to solve this problem. In each step, we minimize $\{Y_s\}_{s=1}^m$ first and then minimize $\{\mu_s\}_{s=1}^m$. We want to show that when the parameter W is fixed, by alternatively minimizing $\{Y_s\}_{s=1}^m$ and $\{\mu_s\}_{s=1}^m$, the energy will converge to the optimal value.

We can easily get the updating rule for $\{Y_s\}_{s=1}^m$ and $\{\mu_s\}_{s=1}^m$ by taking the derivative of the energy function. Note that we always first update $\{Y_s\}_{s=1}^m$ and then update $\{\mu_s\}_{s=1}^m$. For $\{Y_s\}$, we have

$$Y_s^{(k)} = [(1 + \gamma)I + \lambda L_s]^{-1} [f(X_s; W) + \gamma \mu_s^{(k-1)}] \quad (14)$$

For $\{\mu_s\}_{s=1}^m$, we have the i -th row of $\mu_s^{(k)}$ is

$$\mu_{s,i}^{(k)} = \frac{1}{r_{s,i}} \sum_{s'=1}^m \sum_{j=1}^{n'_s} Y_{s',j}^{(k)} \cdot \mathbb{I}\{I(s,i) = I(s',j)\} \quad (15)$$

In another word, the updated $\mu^{(k)}$ is the average of the embeddings of the same node in different subgraphs.

Note that here $\{Y_s\}$ with $\{\mu_s\}$ and \mathbb{Y} with M are used simultaneously. We will use $\{Y_s\}$ and $\{\mu_s\}$ when we want to emphasize the subgraphs and use \mathbb{Y} and M when we want to emphasize them as the input of the global energy function. But in essence they represent the same variables and can be constructed from each other.

The three-point property and four-point property call for a non-negative valued helper function $\delta(Y, Y')$ such that $\delta(Y, Y) = 0$. We define the helper function as $\delta(Y, Y') = (1 + \gamma)\|Y - Y'\|_F^2$. We can easily verify that $\delta(Y, Y) = 0$ and $\delta(Y, Y') \geq 0$.

Lemma D.5 (Three-point property). *Suppose that we have a series of $\mathbb{Y}^{(k)}$ and $M^{(k)}$, $k = 0, 1, 2, \dots$ constructed following the updating rule (14) and (15) and that they are initialized arbitrarily. For any \mathbb{Y} and k , $\ell_{\text{muse}}(\mathbb{Y}, \mu^{(k)}) - \ell_{\text{muse}}(\mathbb{Y}^{(k+1)}, \mu^{(k)}) \geq \delta(\mathbb{Y}, \mathbb{Y}^{(k+1)})$ holds true.*

Proof. We only need to show $\ell_{\text{muse}}^s(Y_s, \mu_s^{(k)}) - \ell_{\text{muse}}^s(Y_s^{(k+1)}, \mu_s^{(k)}) \geq \delta(Y_s, Y_s^{(k+1)})$. By iterating s from 1 to

m and adding the m inequalities together, we can get the desired result.

$$\begin{aligned}
& \ell_{\text{muse}}(Y_s, \mu_s^{(k)}) - \ell_{\text{muse}}(Y_s^{(k+1)}, \mu_s^{(k)}) - \delta(Y_s, Y_s^{(k+1)}) \\
&= \|Y_s - f(X_s; W)\|_F^2 + \lambda \text{tr}(Y_s^\top L_s Y_s) + \gamma \left\| Y_s - \mu_s^{(k)} \right\|_F^2 - \left\| Y_s^{(k+1)} - f(X_s; W) \right\|_F^2 \\
&\quad - \lambda \text{tr}(Y_s^{(k+1)\top} L_s Y_s^{(k+1)}) - \gamma \left\| Y_s^{(k+1)} - \mu_s^{(k)} \right\|_F^2 - (1 + \gamma) \left\| Y_s - Y_s^{(k+1)} \right\|_F^2 \\
&= \left\| Y_s - Y_s^{(k+1)} + Y_s^{(k+1)} - f(X_s; W) \right\|_F^2 + \lambda \text{tr}(Y_s^\top L_s Y_s) \\
&\quad + \gamma \left\| Y_s - Y_s^{(k+1)} - Y_s^{(k+1)} - \mu_s^{(k)} \right\|_F^2 - \left\| Y_s^{(k+1)} - f(X_s; W) \right\|_T^2 \\
&\quad - \lambda \text{tr}(Y_s^{(k+1)\top} L_s Y_s^{(k+1)}) - \gamma \left\| Y_s^{(k+1)} - \mu_s^{(k)} \right\|_F^2 - (1 + \gamma) \left\| Y_s - Y_s^{(k+1)} \right\|_F^2 \\
&= 2 \left\langle Y_s - Y_s^{(k+1)}, Y_s^{(k+1)} - f(X_s; W) \right\rangle + 2\gamma \left\langle Y_s - Y_s^{(k+1)}, Y_s^{(k+1)} - \mu_s^{(k)} \right\rangle \\
&\quad + \lambda \text{tr}(Y_s^\top L_s Y_s) - \lambda \text{tr}(Y_s^{(k+1)\top} L_s Y_s^{(k+1)}) \\
&= 2 \left\langle Y_s - Y_s^{(k+1)}, (1 + \gamma) Y_s^{(k+1)} - (f(X_s; W) + \gamma \mu_s^{(k)}) \right\rangle \\
&\quad + \lambda \left\langle Y_s - Y_s^{(k+1)}, L_s (Y_s + Y_s^{(k+1)}) \right\rangle \\
&= \left\langle Y_s - Y_s^{(k+1)}, 2(\lambda L_s + (1 + \gamma) I) Y_s^{(k+1)} - 2(f(X_s; W) + \gamma \mu_s^{(k)}) + \lambda L_s (Y_s - Y_s^{(k+1)}) \right\rangle \\
&= \left\langle Y_s - Y_s^{(k+1)}, \lambda L_s (Y_s - Y_s^{(k+1)}) \right\rangle \geq 0
\end{aligned}$$

□

Lemma D.6 (four-point property). *Suppose that we have a series of $\mathbb{Y}^{(k)}$ and $M^{(k)}$, $k = 0, 1, 2, \dots$ constructed following the updating rule (14) and (15) and that they are initialized arbitrarily. For any \mathbb{Y} , μ and k , $\delta(\mathbb{Y}, \mathbb{Y}^{(k)}) \geq \ell_{\text{muse}}(\mathbb{Y}, \mu^{(k)}) - \ell_{\text{muse}}(\mathbb{Y}, \mu)$ holds true.*

Proof. Expanding all the functions we can get our target is equivalent to

$$\sum_{s=1}^m (1 + \gamma) \left\| Y_s - Y_s^{(k)} \right\|^2 \geq \gamma \sum_{s=1}^m \left(\left\| Y_s - \mu_s^{(k)} \right\|_F^2 - \|Y_s - \mu_s\|_F^2 \right)$$

We can actually show a stronger result, that is

$$\sum_{s=1}^m \left\| Y_s - Y_s^{(k)} \right\|_F^2 \geq \sum_{s=1}^m \left(\left\| Y_s - \mu_s^{(k)} \right\|_F^2 - \|Y_s - \mu_s\|_F^2 \right)$$

By the updating rule for μ_s , we have

$$\begin{aligned}
& \sum_{s=1}^m \left\langle \mu_s - \mu_s^{(k)}, \mu_s^{(k)} - Y_s^{(k)} \right\rangle \\
&= \sum_{s=1}^m \sum_{i=1}^{n_s} \left\langle \mu_{s,i} - \mu_{s,i}^{(k)}, \mu_{s,i}^{(k)} - Y_{s,i}^{(k)} \right\rangle \\
&= \sum_{v=1}^n \sum_{s=1}^m \sum_{i=1}^{n_s} \mathbb{I}\{I(s, i) = v\} \left\langle M_v - M_v^{(k)}, M_v^{(k)} - Y_{s,i}^{(k)} \right\rangle \\
&= \sum_{v=1}^n r_v \left\langle M_v - M_v^{(k)}, M_v^{(k)} - \frac{1}{r_v} \sum_{s=1}^m \sum_{i=1}^{n_s} \mathbb{I}\{I(s, i) = v\} Y_{s,i}^{(k)} \right\rangle \\
&= 0
\end{aligned} \tag{16}$$

Therefore,

$$\begin{aligned}
& \sum_{s=1}^m \left\| Y_s - Y_s^{(k)} \right\|_F^2 \\
&= \sum_{s=1}^m \left(\|Y_s - \mu_s\|_F^2 + \left\| \mu_s - Y_s^{(k)} \right\|_F^2 + 2 \left\langle Y_s - \mu_s, \mu_s - Y_s^{(k)} \right\rangle \right) \\
&= \sum_{s=1}^m \left(\|Y_s - \mu_s\|_F^2 + \left\| \mu_s - \mu_s^{(k)} \right\|_F^2 + \left\| \mu_s^{(k)} - Y_s^{(k)} \right\|_F^2 \right. \\
&\quad \left. + 2 \left\langle Y_s - \mu_s, \mu_s - Y_s^{(k)} \right\rangle \right) + \sum_{s=1}^m 2 \left\langle \mu_s - \mu_s^{(k)}, \mu_s^{(k)} - Y_s^{(k)} \right\rangle \\
&\stackrel{(16)}{=} \sum_{s=1}^m \left(2 \|Y_s - \mu_s\|_F^2 + \left\| Y_s - \mu_s^{(k)} \right\|_F^2 + \left\| \mu_s^{(k)} - Y_s^{(k)} \right\|_F^2 \right) \\
&\quad + 2 \sum_{s=1}^m \left(\left\langle Y_s - \mu_s, \mu_s - Y_s^{(k)} \right\rangle + \left\langle \mu_s - Y_s, Y_s - \mu_s^{(k)} \right\rangle \right) \\
&= \sum_{s=1}^m \left(2 \|Y_s - \mu_s\|_F^2 + \left\| Y_s - \mu_s^{(k)} \right\|_F^2 + \left\| \mu_s^{(k)} - Y_s^{(k)} \right\|_F^2 \right) \\
&\quad + \sum_{s=1}^m \left(-2 \|Y_s - \mu_s\|_F^2 + 2 \left\langle Y_s - \mu_s, \mu_s^{(k)} - Y_s^{(k)} \right\rangle \right) \\
&= \sum_{s=1}^m \left(\left\| Y_s - \mu_s^{(k)} \right\|_F^2 + \left\| \mu_s^{(k)} - Y_s^{(k)} \right\|_F^2 + 2 \left\langle Y_s - \mu_s, \mu_s^{(k)} - Y_s^{(k)} \right\rangle \right) \\
&= \sum_{s=1}^m \left(\left\| Y_s - \mu_s^{(k)} \right\|_F^2 + \left\| \mu_s^{(k)} - Y_s^{(k)} + Y_s' - \mu_s \right\|_F^2 - \|Y_s - \mu_s\|_F^2 \right) \\
&\geq \sum_{s=1}^m \left(\left\| Y_s - \mu_s^{(k)} \right\|_F^2 - \|Y_s - \mu_s\|_F^2 \right)
\end{aligned}$$

□

Theorem 5.3. Assume $\zeta(y) = 0$. Suppose we have a series of $\mathbb{Y}^{(k)}$ and $M^{(k)}$, $k = 0, 1, 2, \dots$ constructed following the updating rule (14) and (15), with $\mathbb{Y}^{(0)}$ and $M^{(0)}$ initialized arbitrarily. Then

$$\lim_{k \rightarrow \infty} \ell_{muse}(\mathbb{Y}^{(k)}, M^{(k)}) = \inf_{\mathbb{Y}, M} \ell_{muse}(\mathbb{Y}, M),$$

Proof. By Lemma D.5 and Lemma D.6 where both the three-point and four-point property hold true, the theorem is obtained according to Csiszár and Tusnády [1984]. □